

OPEN

Wide-band Beam-scanning by Surface Wave Confinement on Leaky Wave Holograms

Mohammad Moein Moeini¹, Homayoon Oraizi¹, Amrollah Amini¹ & Vahid Nayyeri²

A two-dimensional (2-D) metasurface design for backward leaky wave suppression in microwave regime is proposed based on the theory of holography. The so-called Rabbit's ears phenomenon describes that the backward mode in the reference wave plays the destructive role and makes the holography principle to behave properly mainly in an only narrow frequency interval. Here, we explore the utilization of the surface wave reflectors to suppress the backward mode to achieve wide-band holograms. Therefore, the reference wave form is manipulated by the choice of various reflector shapes and some providing forward mode dominant reference wave are analyzed and simulated. The less backward mode participates in the reference wave; the wider operation frequency range is obtained. With the canceled Rabbit's ears phenomenon, variations in the reference wave frequency cause elevation angle scan. The results provide general insights into relation of the Rabbit's ears phenomenon and the object wave accuracy in frequencies except the design frequency. The idea is also applied to multiple object wave holograms. The concept is verified using both electromagnetic full-wave simulations and experimental measurements.

Controlling electromagnetic waves by the aid of metamaterials and metasurfaces has recently paved the way of beam manipulation in a more modern way¹. Metasurfaces provide the integrability of the electronic components due to the planar shape. This brings degrees of freedom for wave direction^{2–4} and polarization manipulation⁵ and other certain applications like focusing⁶, wave routing⁷ and scattered wave engineering⁸.

Surface wave leakage manipulation is one of the important applications of the metasurfaces. In physics of electromagnetic wave, decrease in amplitude of propagating wave in a lossless medium is associated with energy leakage out of the propagation medium. The propagation medium can be waveguide with metallic boundary, dielectric slab, metasurface waveguide, spoof surface plasmon polariton (SSPP) waveguide and etc. Wave leakage can be brought into play by local perturbation in the propagation medium. The key advantage of the leaky wave systems is the ability of control on the amplitude and propagation direction of the leaky waves⁹. Holography principle for metasurface design is a powerful tool for wave manipulation in any desired direction. The theory of optical holography was first described by Gabor¹⁰, and then the theory was suggested to be utilized in microwave regime by Chaccacci¹¹. Leaky wave hologram capability was verified for pattern synthesis in a desired direction first by Sievenpiper¹². Periodic grounded patches supporting TM_0 surface wave are used to realize this concept. The possibility of polarization manipulation using proper surface impedance distribution has been verified and a new degree of freedom has been added to hologram designs using anisotropic unit-cells^{13,14}. One of the key advantages of the leaky wave structures is the scan capability which can be implemented for Frequency Modulated Continuous Wave (FMCW) systems. Therefore, wide-band operation is a valuable property of leaky wave metasurfaces. However, for 2-D leaky wave metasurfaces designed using holography, pleasant beamforming can be achieved at a single frequency only. Some approaches have been suggested to improve the operating frequency in recent literature. For instance, an increase in bandwidth can be obtained by layering the substrate¹⁵. However, side lobe level (SLL) is not acceptable at higher frequencies. In another work, 1-D scanning angle from -19° to 12° at frequency interval 14–20 GHz is reported by Cu¹⁶. One solution is to locate the wave launcher at corner of the hologram¹⁷. Another is to sectorize the hologram for the launcher power conversion

¹School of Electrical Engineering, Iran University of Science and Technology, 1684613114, Tehran, Iran. ²Antenna and Microwave Research Laboratory and School of New Technologies, Iran University of Science and Technology, 1684613114, Tehran, Iran. Correspondence and requests for materials should be addressed to M.M. (email: mohammad_moeini@elec.iust.ac.ir)

into multi-beam radiation¹⁸. Nevertheless, to achieve high beam directivity at a desired direction and low edge diffraction, utilization of 2-D center-fed leaky wave metasurfaces seems inevitable for practical implementation.

In this work, reflector-enabled 2-D holograms are proposed for wide-band beamforming and scannability. The presence of reflector on metasurface structures may seem to have priority from two point of views; the reflector may contribute in radiation characteristics enhancement, or in some cases, the presence of a reflector as an obstacle is inevitable like vehicular and satellite antennas. Lack of acceptable radiation directivity and bandwidth in center-fed hologram is caused due to a destructive effect called Rabbit's ear phenomenon¹⁷. In 2-D holographic radiators, the radiation corresponding to the forward and backward modes play a constructive role only at design frequency. In fact, the scanning steps for the forward and backward modes are only equal at the design frequency. By placing a reflector on the hologram, backward mode distribution can be changed to eliminate the Rabbit's ear phenomenon. The surface impedance distribution and the corresponding reference wave must be modified to scatter the desired object wave after placing the reflector. The modified impedance is depending on the geometry of the wave reflector placed on the hologram. Radiation characteristics and scannability by frequency may also be enhanced even for multi-beam structures. We propose the surface wave confinement on holographic metasurfaces using surface scatterers which can cancel out the Rabbit's ears phenomenon in a more beneficial way than the previous reflector-free works. As the following explorations prove, surface wave confinement on hologram causes considerable improved radiation bandwidth and scannability for single and multi-beam holograms. The proposed reflector-enabled hologram can achieve single-beam frequency scanning between 13–19 GHz (representing 37.5% fractional bandwidth) and multi-beam frequency scanning between 14–18 GHz (25% fractional bandwidth).

The Theory of Holography in Microwave Regime

Based on the theory of holography, a desired wave profile is produced by exciting the hologram with needed excitation wave. The desired and excitation waves are called object wave (ψ_{obj}) and reference wave (ψ_{ref}), respectively. The recorded interference of reference and object waves called interferogram can project the object wave while it is excited by the reference wave^{19,20}. The concept has laid the foundations for holographic wave manipulation in both optical and microwave regimes. Metasurfaces emulate the interferograms holographic application in microwave. Leaky wave holographic metasurfaces are formed from quasi-periodic surface impedance. In this case, the surface impedance needed for object wave production is defined as

$$Z_s = jX_0\eta_0(1 + M \times \Re\{\psi_{ref}^* \psi_{obj}\}) \quad (1)$$

where X_0 and M represent normalized impedance with respect to the free-space impedance (η_0) and modulation factor, respectively. \Re denotes the real part of a complex value. The reference wave can be chosen as whether space-propagating or surface wave. The reference wave for our desired application is defined as a surface wave in a form of Hankel function of the second kind as

$$\psi_{ref} = a_0 H_0^{(2)}(\beta \sqrt{x^2 + y^2}) \quad (2)$$

where β is the phase constant for the TM_0 surface mode and is obtained as

$$\beta = k_0 \sqrt{1 + X_0^2} \quad (3)$$

Note that the value of β is an approximation of the wave number which is utilized for the object wave calculation and derivation of the associated surface impedance. The approximated value of β is valid when M is small enough²¹. In case that the modulation depth is not small, β should be calculated using the dispersion relation which will be proposed later in this paper. The object wave of interest in this work is a plane wave propagating in a certain direction as

$$\psi_{obj} = e^{-j(kx \sin \theta_0 \cos \phi_0 + ky \sin \theta_0 \sin \phi_0)} \quad (4)$$

Figure 1a represents a typical radiative metasurface using holographic surface impedance (interferogram) for beamforming. Here θ_0 and ϕ_0 are the spherical angles for the object wave propagation direction. The hologram uses cylindrical surface wave to excite the surface impedance to form the object wave. The precise knowledge of 2-D surface impedance distribution is crucial for accurate holographic beamforming. For instance, Fig. 1b shows a 2-D surface impedance distribution aimed to produce an object wave at $\theta_0 = 60^\circ$ and $\phi_0 = 90^\circ$ while it is excited by the reference wave given in (2). The surface impedance is calculated using (1). The color bar on the right shows the imaginary value of the surface impedance for the sample from minimum to maximum.

Rabbit's Ears Phenomenon in Holographic Metasurfaces. In this section, we start the holographic analysis by a center-fed mono-dimensional hologram to illustrate the situation. The reference and object waves are chosen as $\psi_{ref} = e^{-j\beta|x|}$ and $\psi_{obj} = e^{-jk_0 \sin \theta_0 x}$, where β is the real part of the fundamental wave number tangential to the surface impedance κ ($\kappa = \beta - j\alpha$) and α is the attenuation factor along the leaky wave metasurface. In this case, the reference wave on positive and negative directions of x axis are called forward and backward surface leaky modes, respectively. According to (1), the surface impedance Z_s can be expressed as

$$Z_s = jX_0(1 + M \cos(\beta|x| - k_0 \sin \theta_0 x)) \quad (5)$$

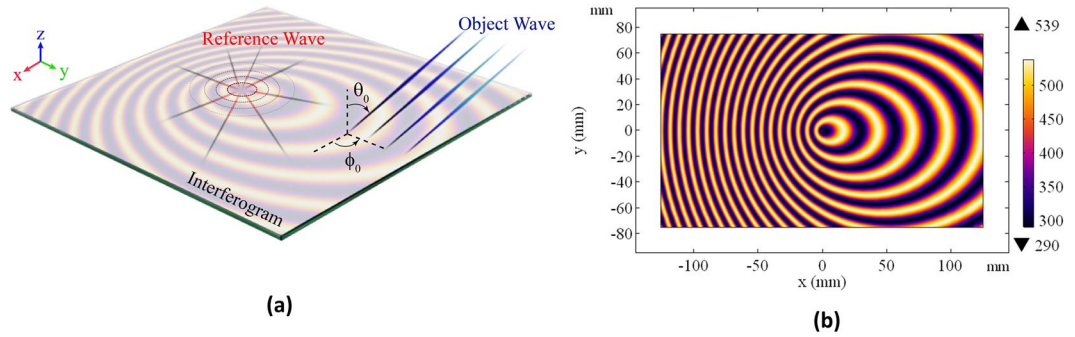


Figure 1. (a) Representation of the reference and object waves. (b) The holographic interference pattern.

For this sinusoidally-modulated surface impedance, the periodicity is

$$d = \frac{2\pi}{\beta - \frac{x}{|x|}k_0 \sin \theta_0} \tag{6}$$

To specify d , the expression for β should be known. The dispersion equation can be written in continued fraction form²²:

$$1 - \frac{j\eta_0}{X_0} \sqrt{1 - \left(\frac{\kappa}{k_0}\right)^2} = \frac{M^2}{4} \left\{ \frac{1}{1 - \frac{j\eta_0}{X_0} \sqrt{1 - \left(\frac{\kappa}{k_0} + \frac{2\pi(-1)}{k_0 a}\right)^2}} - \frac{M^2/4}{\left| 1 - \frac{j\eta_0}{X_0} \sqrt{1 - \left(\frac{\kappa}{k_0} + \frac{2\pi(-2)}{k_0 a}\right)^2} \right|} - \dots + \frac{1}{1 - \frac{j\eta_0}{X_0} \sqrt{1 - \left(\frac{\kappa}{k_0} + \frac{2\pi(1)}{k_0 a}\right)^2}} - \frac{M^2/4}{\left| 1 - \frac{j\eta_0}{X_0} \sqrt{1 - \left(\frac{\kappa}{k_0} + \frac{2\pi(2)}{k_0 a}\right)^2} \right|} - \dots \right\} \tag{7}$$

The typical dispersion diagram of the forward and backward surface wave phase constants for a symmetrical surface impedance (equal periods on forward and backward regions) is shown in Fig. 2a. The diagram indicates that a center-fed leaky wave metasurface with equal surface impedance periods for forward and backward regions is not capable of beamforming at a single direction because the leaky waves from forward and backward surface waves propagating at different directions.

Equation (6) shows that for a leaky wave metasurface designed to radiate toward a direction in the upper half-space ($0^\circ < \theta_0 < 90^\circ$), the period of the modulated surface impedance is shorter on the backward leaky mode region relative to the forward leaky mode region. Figure 2b represents the dispersion diagram for a center-fed leaky wave 1-D surface impedance designed to produce a tilted object wave with respect to the normal vector to the metasurface plane using (5). Considering the asymmetrical surface impedance distribution on each side of the surface wave feed, as it is shown in Fig. 2b, the dispersion curves corresponding to each forward and backward modes cross at β_0 which is associated with design frequency f_0 . In other words, only identical β for the forward and backward leaky waves make the radiated object waves to participate in a constructive manner by propagation in a single direction. Therefore, to design a conventional bilateral hologram, it is necessary for the forward and backward regions surface impedance periods to be chosen in a way that the dispersion curves cross each other at (f_0, β_0) . Any variation in frequency makes the β_f (forward leaky wave phase constant) and β_b (backward leaky wave phase constant) to separate from β_0 on the dispersion diagram. Therefore, the θ_f and θ_b deviate from each other. At frequency $f_0 - \delta f$, the forward and backward modes' angles with respect to the normal direction are $\theta_f - \delta\theta_f$ and $\theta_b + \delta\theta_b$, respectively. Thus, at any other frequency except f_0 , the total radiation pattern is not acceptable. This destructive effect on the object wave is called Rabbit's ears phenomenon¹⁷. Figure 2c,d illustrate the operation frequency restriction of radiative leaky wave antennas. They show the leaky wave directions of forward and backward modes at the design frequency f_0 and $f_0 - \delta f$.

This concept may be generalized to a 2-D hologram (see Fig. 3). Assuming the object wave as a pencil beam directed in γ_0 with respect to x axis at f_0 , two hypothetical lines L_0 and L_1 are projected on the metasurface which are located at Φ_0 and Φ_1 , respectively. Unit-cells (realized surface impedance) on the metasurface which are along

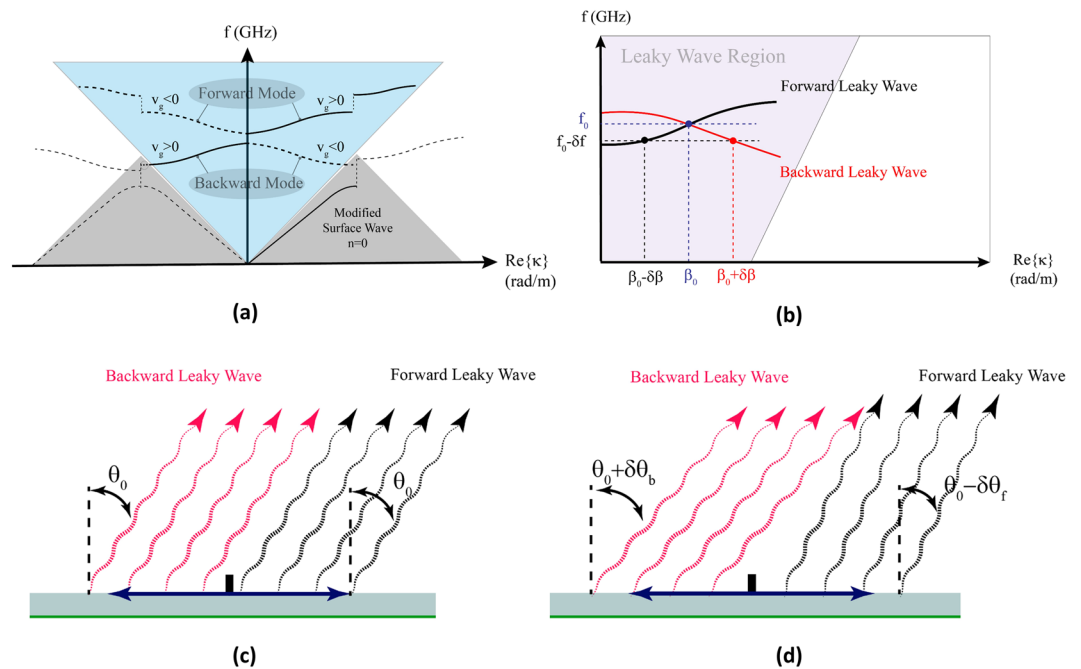


Figure 2. Comparison of the beam angles due to the forward and backward modes on a symmetrical modulated surface impedance. (a) Typical dispersion diagram of the 1-D leaky wave structure for periodic small perturbations. (b) Dispersion comparison between the forward and backward leaky wave modes at the design frequency (f_0) and a slightly lower than the design frequency sample ($f_0 - \delta f$) on an asymmetrical surface impedance. Propagation directions illustration of forward and backward leaky waves at (c) f_0 and (d) $f_0 - \delta f$ operation frequencies.

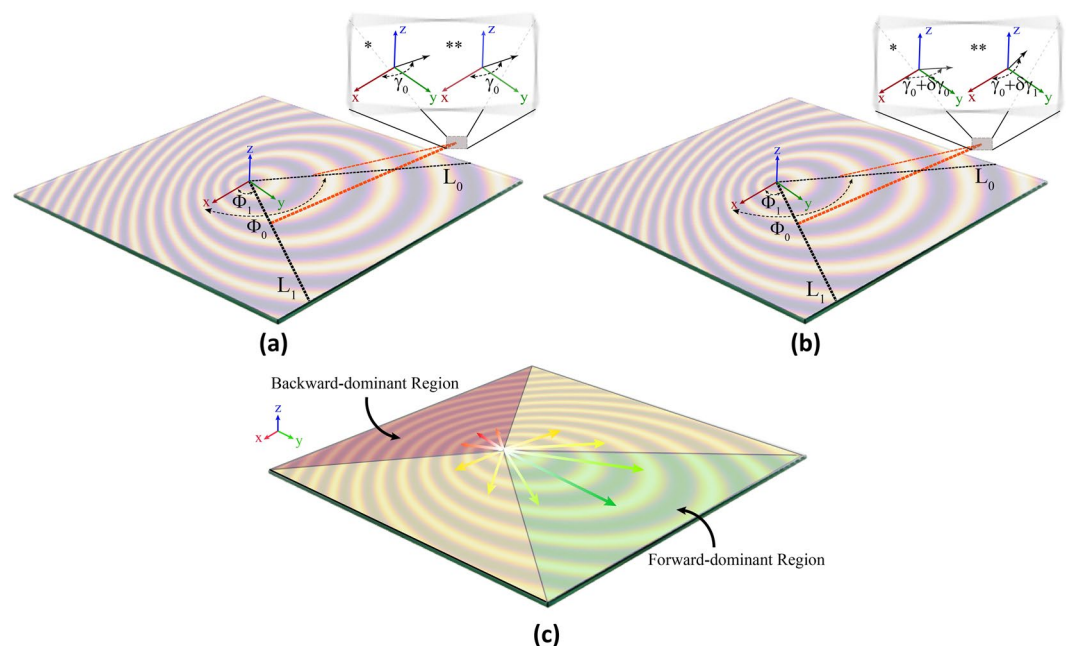


Figure 3. (a) Hologram operation at f_0 , (b) Hologram operation at $f_0 - \delta f$. The single star (*) is for the beam generated by surface wave along L_0 and double star (**) is for the beam generated by surface wave along L_1 . (c) The regions on the metasurface including the forward-dominant and backward-dominant regions for a tilted object wave generation using a center-fed cylindrical surface wave launcher.

L_0 and L_1 both contribute to produce the object wave in γ_0 direction at f_0 . If the frequency is shifted from f_0 , the scanning direction and surface impedance step corresponding to the unit-cells along L_0 and L_1 will be different from each other. Hence, at $f_0 - \delta f$, the leaky waves produced by the unit-cells along L_0 and L_1 propagate in dif-

ferent directions. Therefore, the Rabbit's ears phenomenon occurs and beamforming at a single direction is impossible when frequency is shifted from the desired frequency f_0 (Fig. 3b).

It can be concluded from the above discussion that for a distortion-free radiation pattern over a frequency interval, a backward mode suppression is essential. Apart from mathematics, for a hologram aimed to generate a tilted object wave through Y-Z plane, an overall deduction can be generalized from Fig. 3c that the more surface wave vectors seem alike with a y-directed surface wave, the less destructive effect occurs. In other words, the green arrows represent the most constructive case, while the red ones represent the most destructive case. We propose confinement of the surface wave using reflectors. Therefore, a proper selection of surface wave reflector geometry may cause surface wave confinement to the forward-dominant region. The surface wave confinement into forward mode radiating section eliminates the backward mode destructive effect.

Leak Wave Holography in Presence of Surface Wave Reflector

Single Object Wave. Monopole launcher on a grounded dielectric is a proper choice for TM_0 surface wave production. The electric and magnetic fields of the monopole launcher with moment $I_0\Delta z$ in a cylindrical coordinate can be written as¹³

$$\vec{E}_{sw} = \left[jX_s J_{sw} H_1^{(2)}(\beta\rho) \hat{\rho} + J_{sw} \frac{\beta\eta_0}{k_0} H_0^{(2)}(\beta\rho) \hat{z} \right] e^{-\alpha_z z} \tag{8}$$

$$\vec{H}_{sw} = -J_{sw} H_1^{(2)}(\beta\rho) e^{-\alpha_z z} \hat{\phi} \tag{9}$$

where β and α_z are the phase constant in the propagation direction and the attenuation constant in the z direction, respectively. X_s is the positive surface reactance of the grounded dielectric and J_{sw} is defined²³

$$J_{sw} = -I_0\Delta z \frac{k_0\beta X_s}{2} \tag{10}$$

With the aid of the Poynting's vector, the power carrying by above fields is

$$\begin{aligned} \vec{S}_{sw} &= \vec{E}_{sw} \times \vec{H}_{sw}^* \\ &= -jX_s |J_{sw}|^2 |H_1^{(2)}(\beta\rho)|^2 e^{-2\alpha_z z} \hat{z} \\ &\quad + \frac{\eta_0\beta}{k_0} |J_{sw}|^2 H_0^{(2)}(\beta\rho) H_1^{(2)*}(\beta\rho) e^{-j2\alpha_z z} \hat{\rho} \end{aligned} \tag{11}$$

The z component of the Poynting's vector is pure imaginary demonstrating that the power does not leave the dielectric slab along the z direction, i.e. the power density only surges up and down with no propagation²⁴. In other words, the z -directed power density is stored and the propagation occurs only in ρ direction. The imaginary part of the Poynting's vector exist at ρ and z directions which represents the coupling of the wave to the dielectric. The real part also explains wave propagation in ρ direction and this part only impresses contribution in holography equation (1). Therefore, the reference wave can properly be designated as zero order Hankel function of the second kind.

Let us consider an infinitely long conducting wire within a medium with refractive index $n = \sqrt{1 + X_0^2}$. If the wire is directed along the z axis, the radiated electric and magnetic fields are in the z and ϕ directions, respectively and can be written as²⁵

$$E_z = -I_e \frac{\omega\mu}{4} H_0^{(2)}(\beta\rho) \tag{12}$$

$$H_\phi = -jI_e \frac{\beta}{4} H_1^{(2)}(\beta\rho) \tag{13}$$

where I_e is a constant. Comparing (12) with (8) and (13) with (9), it can be concluded that the monopole wave launcher and long conducting wire represent an equivalent wave function at $z = 0$ on the metasurface.

As mentioned before, the Rabbit's ears phenomenon leads to a destructive effect on the radiation characteristics of the hologram. To prevent this destruction, we propose using a PEC wall reflector. It can be predicted that the scattering effect of the reflector changes the destructive backward mode into a constructive forward mode which results in improving the radiation characteristics. However, looking back to Fig. 3c, to cancel out the Rabbit's ears phenomenon in 2-D, wedge reflector as a surface wave reflector seems more appropriate. To verify this idea, we need the surface wave function of the cylindrical wave launcher next to the wedge reflector which can be derived analytically. For an infinite conducting wire placed next to a wedge reflector at ρ_0 and ϕ_0 , the total wave expression can be written as²⁵

$$\psi_{ref} = \begin{cases} \sum_{\nu} a_{\nu} J_{\nu}(k\rho) H_{\nu}^{(2)}(k\rho_0) \sin(\nu(\phi - \phi_0)) \sin(\nu(\phi - \zeta)) & \rho < \rho_0 \\ \sum_{\nu} a_{\nu} J_{\nu}(k\rho_0) H_{\nu}^{(2)}(k\rho) \sin(\nu(\phi - \phi_0)) \sin(\nu(\phi - \zeta)) & \rho > \rho_0 \end{cases} \tag{14}$$

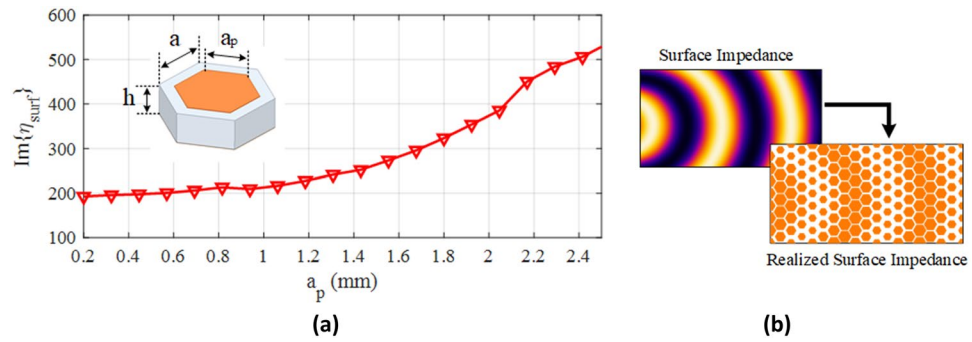


Figure 4. Realization process. (a) Imaginary part of surface impedance for hexagonal metallic patch side lengths. The results are for $a = 2.7$ mm. (b) Assigning different surface impedance values to corresponding metallic patches.

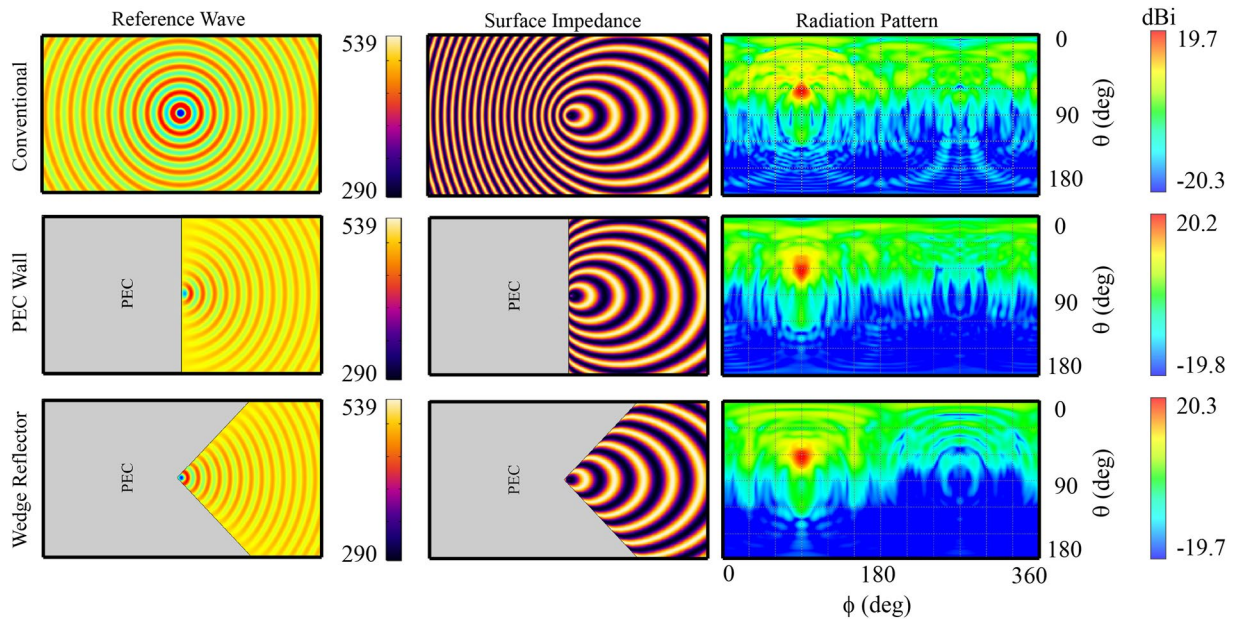


Figure 5. Comparison of reference waves, surface impedances, and 2-D distributed radiation patterns of conventional and reflector-enabled (PEC wall and wedge reflector) holograms all aimed to produce a certain object wave ($\phi_0 = 90^\circ$ and $\theta_0 = 60^\circ$). The simulation results are for the design frequency $f_0 = 18$ GHz.

where $k = nk_0$, ζ is half of the total inner wedge angle, and J_ν represents the Bessel function of the first kind of order ν . Satisfying boundary conditions on the wedge and conducting wire will result ν and a_ν as

$$\nu = \frac{m\pi}{2(\pi - \alpha)} \quad m = 1, 2, 3, \dots \tag{15}$$

$$a_\nu = -\frac{\pi\omega\mu I_e}{2(\pi - \alpha)} \tag{16}$$

With the modified reference wave, the modified surface impedance Z_s must be calculated using holography theorem. The surface impedance is obtained by substituting the reference wave expression (14) into (1) and then the object wave is produced when the newly resulted interferogram is excited by the modified reference wave.

The surface impedance realization requires a unit-cell design to represent the corresponding surface impedance cell obtained from surface impedance discretization. The unit-cell dimensions must be chosen relatively smaller than the operating wavelength of the hologram. Hexagonal unit-cell is proposed for surface impedance realization. The unit-cell with hexagonal lattice shape is more well-behaved considering the dispersion isotropy^{26,27}. Figure 4a shows the hexagonal unit-cell and the surface impedance variations versus the length of the hexagonal side (a_p). The surface impedance is calculated using the equivalent circuit method²¹. Figure 4b shows how the surface impedance is realized by the hexagonal unit-cells.

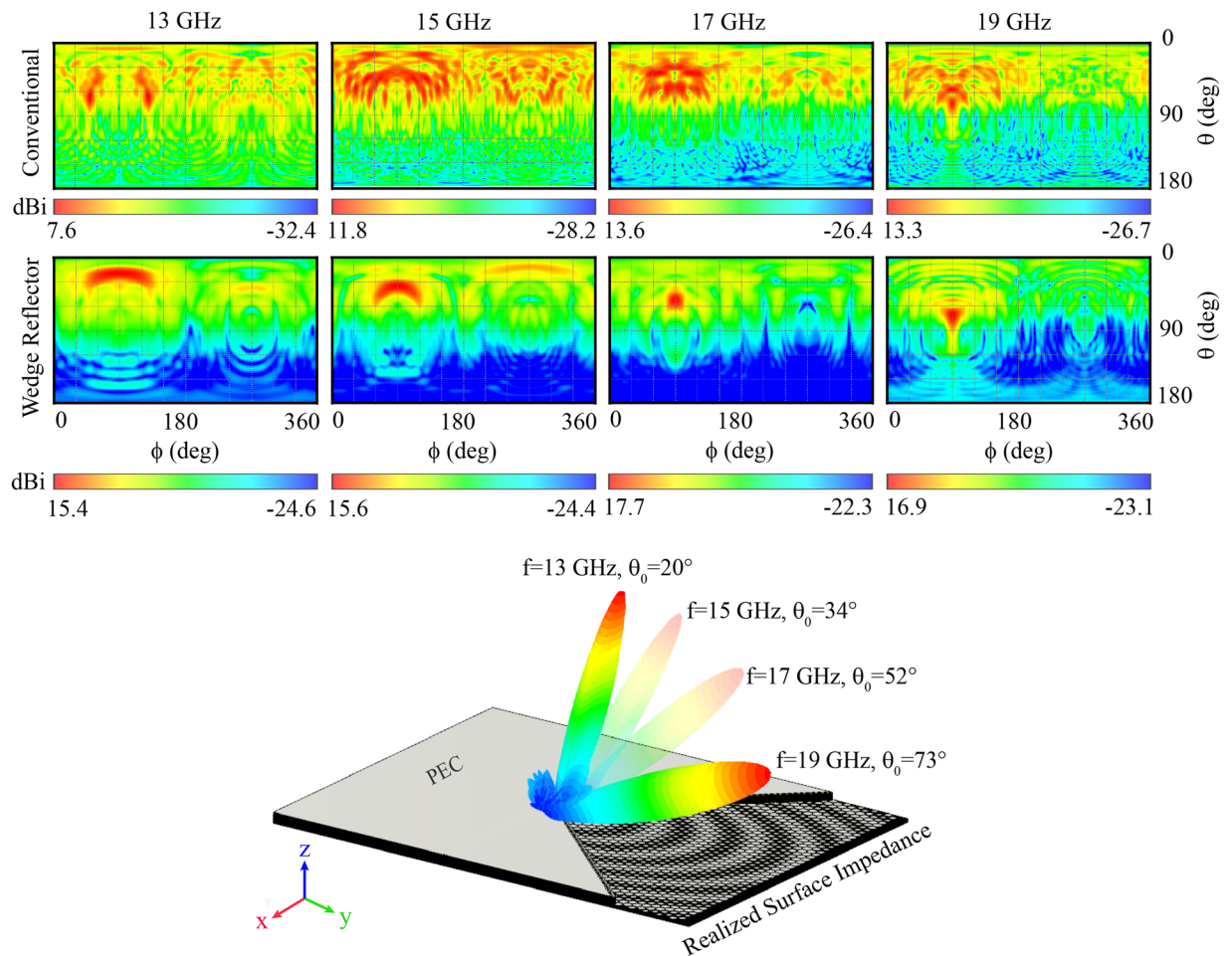


Figure 6. Pattern comparison of conventional hologram and the proposed hologram with wedge reflector. Illustration of the scannability property of the proposed hologram.

Three different leaky wave hologram configurations are compared: conventional hologram (without reflector), a hologram with a PEC wall reflector, and a hologram with a wedge PEC reflector. Figure 5 shows the reference wave, the surface impedance, and the 2-D distributed pattern of each. The surface impedances and 2-D patterns are resulted for the purpose of generating an object wave in $\phi_0 = 0^\circ$ and $\theta_0 = 60^\circ$ direction at $f_0 = 18$ GHz. The directivity for the conventional hologram is obtained 18.3 dB, while for the holograms with PEC wall and wedge reflector the results are 20.2 dB and 20.3 dB at the design frequency 18 GHz, respectively. A relatively low directivity of the conventional hologram at the design frequency f_0 can be attributed to the lack of enough approximation for the shorter surface impedance periods on the backward region of the conventional hologram. The rapid surface impedance variations on the backward region require higher 2-D discretization rate relative to the surface impedance on the forward region. Therefore, conventional leaky wave hologram shows high fabrication demands for realizing surface impedance on the backward region. The backward surface waves in reflector-enabled structures are redirected into forward region. The surface impedance on the reflector-enabled holograms are made of longer periods compared to the backward region of conventional hologram, as seen in Fig. 5. Thus, an advantage of the proposed reflector-enabled leaky wave holograms is simpler fabrication necessities for realization of unit-cell by elimination of very small unit-cells in the backward region.

Apart from the design frequency f_0 , a superior functional advantage of the reflector-enabled leaky wave holograms occurs. Comparing Figs 3c and 5, the hologram with wedge reflector seems to confine the surface waves into forward-dominant region more efficiently and less Rabbit's ears phenomenon is predicted for this structure when the operating frequency is shifted from f_0 . It is known that at frequencies other than f_0 , the backward and forward leaky waves directions deviate. However, there is no backward leaky wave for the hologram with wedge reflector and all the reflected surface wave contribute to object wave construction as forward mode. The result is a single beam with directivity maintenance over a wide frequency range. The peak of the radiation pattern as a function of frequency is given approximately²²

$$\theta_{-1}(f) = \sin^{-1} \left[\frac{\beta + \frac{2\pi(-1)}{d}}{k_0} \right] \quad (17)$$

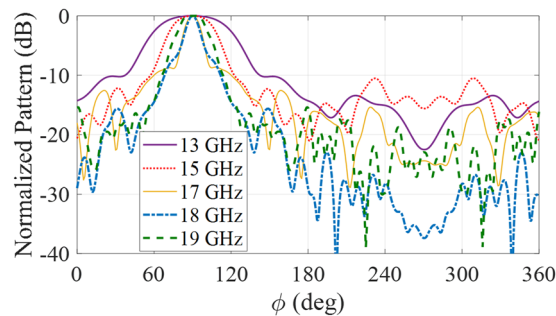


Figure 7. H-plane radiation pattern of wedge-reflector hologram at different frequencies.

where the subscript -1 indicates the dominant spatial harmonic in leaky wave radiators (mode $n = -1$). Therefore, frequency variation causes beam scanning.

Figure 6 depicts the radiation patterns of the conventional and the proposed wedge reflector-supported holograms at different frequencies. Although, as shown in Fig. 5, the conventional hologram forms the desired beam at $f_0 = 18$ GHz, as shown in Fig. 6, the beamforming is not acceptable at nearby frequencies, e.g., 13, 15, 17, and 19 GHz. On the other hand, by applying the proposed wedge reflector-supported hologram, an object wave is formed not only at the design frequency $f_0 = 18$ GHz but also at a wide frequency range. The figure also shows that for the proposed hologram, the progressive variation of frequency changes the object wave radiation direction in a way that the hologram is capable of frequency scanning of elevation angle (θ) from 20° to 73° by varying the frequency over 13–19 GHz. The directivity for surface impedance modulated leaky wave antennas is²⁸:

$$D \propto \frac{\beta_{\perp(-1)}}{\alpha_{\parallel(-1)}} = \frac{\sqrt{\omega^2 \mu_0 \varepsilon_0 - \left[\kappa + \frac{2\pi(-1)}{a} \right]^2}}{\alpha_{\parallel(-1)}} \quad (18)$$

where subscript (-1) , β_{\perp} and α_{\parallel} indicate unbounded propagating mode number, phase constant in normal direction and attenuation constant in parallel direction relative to the metasurface plane, respectively. The modulation factor M determines the surface wave attenuation constant¹⁴. More values for M result more surface wave attenuation and therefore lower directivity. This means that for a forward surface wave leaky wave antenna, due to the nature of leaky wave antennas, the directivity will reduce as the beamforming angle gets close to the broadside angle. Hence, as may be observed from (18), lowering the modulation factor M causes smaller α_{\parallel} . With weak attenuation constant, the leaky wave antenna requires longer propagation path for the desired radiation and larger antenna dimensions seem inevitable. Therefore, the trade-off between directivity and antenna dimensions should always be considered.

In Fig. 7 H-plane patterns of the proposed wedge reflector-enabled antenna are compared from 13 to 19 GHz.

In general, the cross-polarization is low for this type of antenna both in E-plane and H-plane. Figure 8 shows the cross-polarization in E and H planes versus frequency. The cross-polarization is acceptable (less than -30 dB) at the design direction $\theta_0 = 60^\circ$ and $\phi_0 = 90^\circ$. For other azimuth angles, the cross-polarization value is increased due to isotropic unit-cell¹⁴.

Multiple Object Waves. Multi-beam generation by holography requires the summation of each individual object waves making up the total object wave expression. In order to generate object waves directed in (θ_1, ϕ_1) and (θ_2, ϕ_2) , the object wave is defined

$$\psi_{obj} = e^{-j(kx \sin \theta_1 \cos \phi_1 + ky \sin \theta_1 \sin \phi_1)} + e^{-j(kx \sin \theta_2 \cos \phi_2 + ky \sin \theta_2 \sin \phi_2)} \quad (19)$$

Substituting dual-beam object wave expression (19) in (1), the surface impedance needed for dual-beam generation can be obtained. Assuming that the object waves are directed in $\theta_1 = 30^\circ$ and $\theta_2 = 60^\circ$ in z - y plane ($\phi_1 = \phi_2 = 90^\circ$), Fig. 9 shows the holographic surface impedance for such a hologram. The surface impedance is excited using cylindrical surface wave launcher and the reference wave should be updated after reflection from wedge reflector (reference wave expression is 14 again). Operation in wide frequency range was the result of the backward mode suppression for holograms producing single object wave. To illustrate whether the concept is generalizable to multiple object waves, simulations for further frequencies and elevation angle scan are done and can be seen in Fig. 9. Observe that the hologram still keeps scanning the elevation angle in z - y plane as the frequency varies. The difference in object waves' angles does not change by frequency variation and preserves at 30° approximately.

Generating multiple object waves each directed in a direction without complicated feeding network is an attractive application of leaky wave metasurfaces^{17,18}. Leaky wave multidirectional beamforming without holography is a complicated procedure. For instance, one approach is multi-beam pillbox leaky wave antenna based on SIW technology²⁹. The design provides scannability property by frequency variation from 23.5 GHz to 26 GHz with fractional bandwidth of 10%. However, the proposed reflector-enabled hologram can achieve single-beam

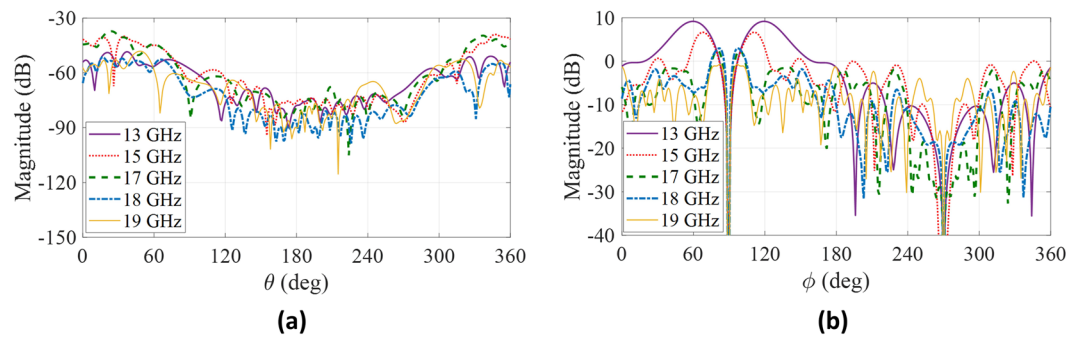


Figure 8. Cross-polarization patterns of the proposed antenna at different frequencies: (a) E-plane. (b) H-plane.

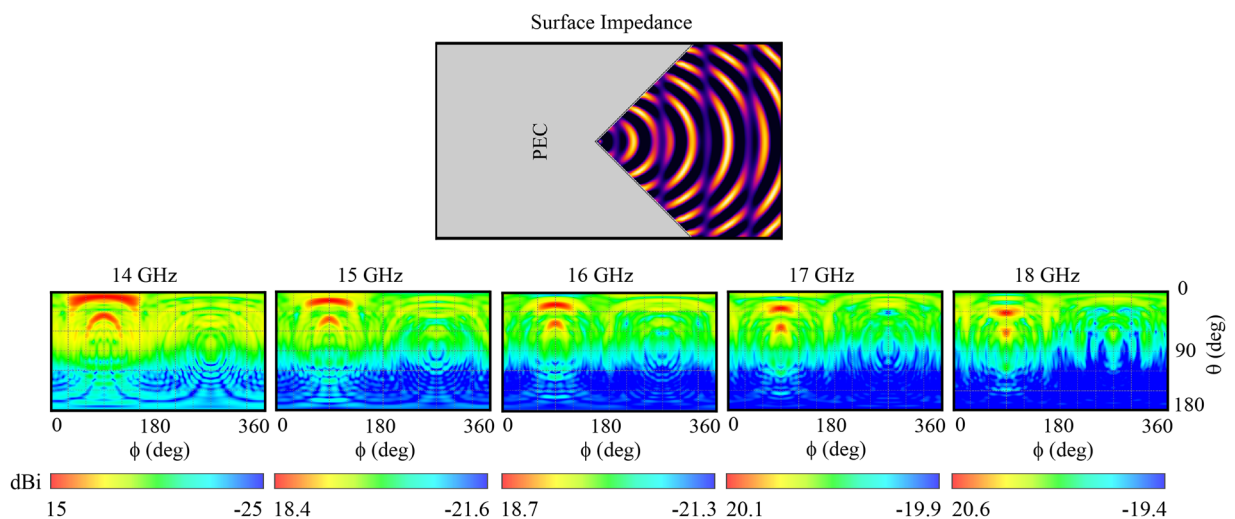


Figure 9. Surface impedance configuration of dual-beam generating metasurface and 2-D distributed radiation patterns of the wide-band dual-beam hologram over 14–18 GHz indicating elevation angle scanning. The simulation result shows two major lobes directed in desired angles at design frequency $f_0 = 18$ GHz.

frequency scanning between 13–19 GHz (representing 37.5% fractional bandwidth) and multi-beam frequency scanning between 14–18 GHz (25% fractional bandwidth).

On the other hand, the conventional microwave holograms operate at a narrow frequency bandwidth. The Rabbit's ears phenomenon cancellation using reflectors can help to obtain an acceptable operating frequency range for holographic multiple object waves beamforming.

Experimental Validation

To experimentally validate the concept, the designed wedge reflector-supported hologram was fabricated which is shown in Fig. 10a. The surface wave launcher should be capable of generating Hankel surface wave over an acceptable frequency range. Among various types of surface wave launchers of this kind, the monopole antenna is a reasonable and simple choice. Since, fabrication of a PEC reflector is not possible using printed circuit board technologies, metalized vias are utilized to simplify the fabrication process. To realize the surface impedance, it has to be discretized and each sample is realized using hexagonal patch which represents the same surface reactance. The radiation pattern of the fabricated holographic antenna was measured in an anechoic chamber as shown in Fig. 10a. Figure 10b shows the simulation and measurement results for the radiation pattern over a frequency range of 13–18 GHz demonstrating an excellent agreement between the simulations and measurements. Both simulation and measurement results indicate the frequency-controlled beams scanning radiation provided by the proposed design.

Conclusion

The Rabbit's ears phenomenon is known for the destructive effect of the forward and backward modes in a center-fed hologram which severely restricts the bandwidth of the design to a single frequency. We proposed reflector-enabled holograms to suppress the backward mode and refine the surface wave distribution in a more constructive manner. We showed theoretically and experimentally that a wedge reflector-supported hologram

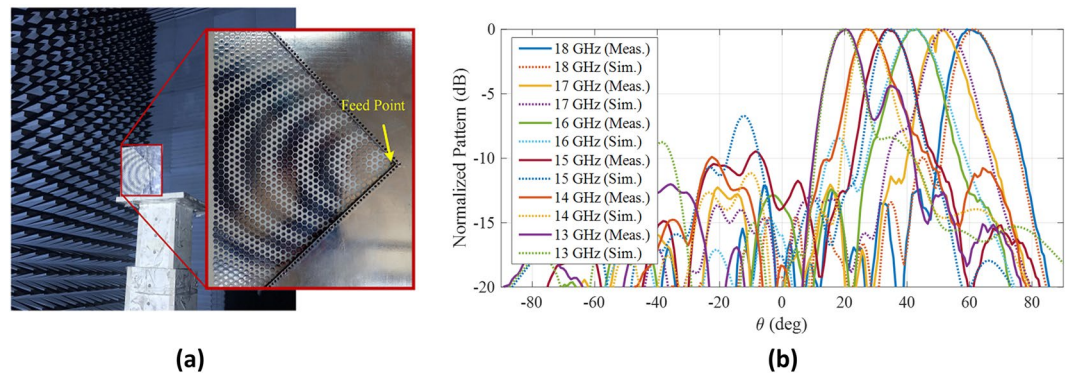


Figure 10. (a) Fabricated prototype of the hologram with wedge reflector. (b) Normalized radiation pattern of the proposed hologram with the wedge reflector at operating frequency range from 13 GHz to 18 GHz. Solid and dashed lines represent simulation and measurement results, respectively.

provides beamforming and beamscanning features in a wide frequency bandwidth. Our simulation results demonstrated that this concept is not limited to single-beam holograms but can be generalized to design of multi-beam holograms. Two reflector shapes were designed to provide a comparison on reference wave distribution. Another discussion showed the wide-band acceptable operation of the hologram with wedge reflector versus some other types of holograms. The capability of scan by frequency variation is resulted for microwave 2-D holograms due to the acceptable operation frequency range. The fact that the forward mode dominant holographic reference wave provides wide frequency band and scannability is also true for multi-beam holograms.

References

- Smith, D. R., Pendry, J. B. & Wiltshire, M. C. K. Metamaterials and negative refractive index. *Science* **305**, 788–792, <https://doi.org/10.1126/science.1096796> (2004).
- Li, Y. B., Cai, B. G., Cheng, Q. & Cui, T. J. Isotropic holographic metasurfaces for dual-functional radiations without mutual interferences. *Advanced Functional Materials* **26**, 29–35, <https://doi.org/10.1002/adfm.201503654>.
- Wan, X., Li, Y. B., Cai, B. G. & Cui, T. J. Simultaneous controls of surface waves and propagating waves by metasurfaces. *Applied Physics Letters* **105**, 121603, <https://doi.org/10.1063/1.4896540> (2014).
- Pfeiffer, C. & Grbic, A. Metamaterial Huygens' surfaces: Tailoring wave fronts with reflectionless sheets. *Phys. Rev. Lett.* **110**, 197401, <https://doi.org/10.1103/PhysRevLett.110.197401> (2013).
- Guo, Y. *et al.* Dispersion management of anisotropic metamirror for super-octave bandwidth polarization. *Scientific Reports* **5**, 1–7 (2015).
- Arbabi, E. *et al.* Mems-tunable dielectric metasurface lens. *Nature Communications* **9**, 1–9 (2018).
- Achouri, K. & Caloz, C. Space-wave routing via surface waves using a metasurface. *Scientific Reports* **8**, 1–9 (2018).
- Momeni, A., Rouhi, K., Rajabalipanah, H. & Abdolali, A. An information theory-inspired strategy for design of reprogrammable encrypted graphene-based coding metasurfaces at terahertz frequencies. *Scientific Reports* **8**, 1–13 (2018).
- Monticone, F. & Alù, A. Leaky-wave theory, techniques, and applications: From microwaves to visible frequencies. *Proceedings of the IEEE* **103**, 793–821, <https://doi.org/10.1109/JPROC.2015.2399419> (2015).
- Gabor, D. A new microscopic principle. *Nature* **161**, 777–778 (1948).
- Checacci, P. F., Russo, V. & Scheggi, A. M. Holographic antennas. *Proceedings of the IEEE* **56**, 2165–2167, <https://doi.org/10.1109/PROC.1968.6832> (1968).
- Fong, B. H., Colburn, J. S., Ottusch, J. J., Visher, J. L. & Sievenpiper, D. F. Scalar and tensor holographic artificial impedance surfaces. *IEEE Transactions on Antennas and Propagation* **58**, 3212–3221, <https://doi.org/10.1109/TAP.2010.2055812> (2010).
- Minatti, G., Caminita, F., Casaletti, M. & Maci, S. Spiral leaky-wave antennas based on modulated surface impedance. *IEEE Transactions on Antennas and Propagation* **59**, 4436–4444, <https://doi.org/10.1109/TAP.2011.2165691> (2011).
- Minatti, G., Caminita, F., Martini, E., Sabbadini, M. & Maci, S. Synthesis of modulated-metasurface antennas with amplitude, phase, and polarization control. *IEEE Transactions on Antennas and Propagation* **64**, 3907–3919, <https://doi.org/10.1109/TAP.2016.2589969> (2016).
- Pandi, S., Balanis, C. A. & Birtcher, C. R. Analysis of wideband multilayered sinusoidally modulated metasurface. *IEEE Antennas and Wireless Propagation Letters* **15**, 1491–1494, <https://doi.org/10.1109/LAWP.2015.2514241> (2016).
- Li, Y. B., Li, L. L., Cai, B. G., Cheng, Q. & Cui, T. J. Holographic leaky-wave metasurfaces for dual-sensor imaging. *Scientific Reports* **5**, 1–7 (2015).
- Li, Y. B., Wan, X., Cai, B. G., Cheng, Q. & Cui, T. J. Frequency-controls of electromagnetic multi-beam scanning by metasurfaces. *Scientific Reports* **4**, 1–7 (2014).
- González-Ovejero, D., Minatti, G., Chattopadhyay, G. & Maci, S. Multibeam by metasurface antennas. *IEEE Transactions on Antennas and Propagation* **65**, 2923–2930, <https://doi.org/10.1109/TAP.2017.2670622> (2017).
- Hariharan, P. *Optical holography, principles, techniques and applications*. 1 (Cambridge University Press, 1996).
- Hariharan, P. *Basics of interferometry*. 1 (Elsevier, 2007).
- Patel, A. M. & Grbic, A. A printed leaky-wave antenna based on a sinusoidally-modulated reactance surface. *IEEE Transactions on Antennas and Propagation* **59**, 2087–2096, <https://doi.org/10.1109/TAP.2011.2143668> (2011).
- Oliner, A. & Hessel, A. Guided waves on sinusoidally-modulated reactance surfaces. *IRE Transactions on Antennas and Propagation* **7**, 201–208, <https://doi.org/10.1109/TAP.1959.1144771> (1959).
- Sarabandi, K., Casciato, M. D. & Koh, I. S. Efficient calculation of the fields of a dipole radiating above an impedance surface. *IEEE Transactions on Antennas and Propagation* **50**, 1222–1235, <https://doi.org/10.1109/TAP.2002.7054733> (2002).
- Elliot, R. *Antenna Theory and Design, Revised Ed* (Wiley India Pvt. Limited, 2006).
- Balanis, C. A. *Advanced Engineering Electromagnetics*. 1 (Wiley, 2012).
- Li, M., Xiao, S. Q. & Sievenpiper, D. F. Polarization-insensitive holographic surfaces with broadside radiation. *IEEE Transactions on Antennas and Propagation* **64**, 5272–5280, <https://doi.org/10.1109/TAP.2016.2618853> (2016).

27. Oraizi, H., Amini, A., Abdolali, A. & Karimimehr, M. Design of wideband leaky wave antenna using sinusoidally modulated impedance surface based on the holography theory. *IEEE Antennas and Wireless Propagation Letters* 1–1, <https://doi.org/10.1109/LAWP.2018.2866712> (2018).
28. Collin, R. E. & Zucker, F. J. *Antenna Theory*. 1 (McGraw-Hill, 1969).
29. Ettorre, M., Sauleau, R. & Le Coq, L. Multi-beam multi-layer leaky-wave siw pillbox antenna for millimeter-wave applications. *IEEE Transactions on Antennas and Propagation* 59, 1093–1100, <https://doi.org/10.1109/TAP.2011.2109695> (2011).

Author Contributions

M.M. and A.A. conceived the idea, developed the theory, did the simulations, and wrote the manuscript. V.N. was involved in the discussions and performed the measurements. V.N. and H.O. analyzed the results and reviewed the manuscript. H.O. supervised the project.

Additional Information

Competing Interests: The authors declare no competing interests.

Publisher's note: Springer Nature remains neutral with regard to jurisdictional claims in published maps and institutional affiliations.



Open Access This article is licensed under a Creative Commons Attribution 4.0 International License, which permits use, sharing, adaptation, distribution and reproduction in any medium or format, as long as you give appropriate credit to the original author(s) and the source, provide a link to the Creative Commons license, and indicate if changes were made. The images or other third party material in this article are included in the article's Creative Commons license, unless indicated otherwise in a credit line to the material. If material is not included in the article's Creative Commons license and your intended use is not permitted by statutory regulation or exceeds the permitted use, you will need to obtain permission directly from the copyright holder. To view a copy of this license, visit <http://creativecommons.org/licenses/by/4.0/>.

© The Author(s) 2019